PNAS RESEARCH ARTICLE | IMMUNOLOGY AND INFLAMMATION

NAD^+ metabolism drives astrocyte proinflammatory reprogramming in central nervous system autoimmunity

Tom Meyer[a,1], Dor Shimon[b,1], Sawsan Youssef[c], Gal Yankovitz[b], Adi Tessler[b], Tom Chernobylsky[b], Anat Gaoni-Yogev[b], Rita Perelroizen[a], Noga Budick-Harmelin[b], Lawrence Steinman[c], and Lior Mayo[a,b,2]

Edited by Harvey Cantor, Dana-Farber Cancer Institute, Boston, MA; received July 1, 2022; accepted July 28, 2022

Multiple sclerosis (MS) is a chronic inflammatory disease of the central nervous system (CNS). Astrocytes are the most abundant glial cells in the CNS, and their dysfunction contributes to the pathogenesis of MS and its animal model, experimental autoimmune encephalomyelitis (EAE). Recent advances highlight the pivotal role of cellular metabolism in programming immune responses. However, the underlying immunometabolic mechanisms that drive astrocyte pathogenicity remain elusive. Nicotinamide adenine dinucleotide (NAD^+) is a vital coenzyme involved in cellular redox reactions and a substrate for NAD^+-dependent enzymes. Cellular NAD^+ levels are dynamically controlled by synthesis and degradation, and dysregulation of this balance has been associated with inflammation and disease. Here, we demonstrate that cell-autonomous generation of NAD^+ via the salvage pathway regulates astrocyte immune function. Inhibition of nicotinamide phosphoribosyltransferase (NAMPT), a key enzyme in the salvage pathway, results in depletion of NAD^+, inhibits oxidative phosphorylation, and limits astrocyte inflammatory potential. We identified CD38 as the main NADase up-regulated in reactive mouse and human astrocytes in models of neuroinflammation and MS. Genetic or pharmacological blockade of astrocyte CD38 activity augmented NAD^+ levels, suppressed proinflammatory transcriptional reprogramming, impaired chemotactic potential to inflammatory monocytes, and ameliorated EAE. We found that CD38 activity is mediated via calcineurin/NFAT signaling in mouse and human reactive astrocytes. Thus, NAMPT–NAD^+–CD38 circuitry in astrocytes controls their ability to meet their energy demands and drives the expression of proinflammatory transcriptional modules, contributing to CNS pathology in EAE and, potentially, MS. Our results identify candidate therapeutic targets in MS.

astrocyte | tryptophan catabolism | neuroinflammation | multiple sclerosis | Nicotinamide adenine dinucleotide

Significance

NAD^+ has emerged as an important cofactor that can rewire metabolism and link energy status with cellular immune response reprogramming, raising the possibility that an improved understanding of NAD^+ immunometabolic function in neuroinflammation could be exploited therapeutically. We have now identified the enzymes NAMPT, CD38, and the transcription factor NFATC3 as critical nodes in regulating astrocyte pathogenicity and controlling experimental neuroinflammation. Importantly, we have corroborated these murine findings in human astrocytes and analysis of MS brain samples. Overall, our results describe the role of NAD^+ metabolism in the local immune response in the CNS and reveal targetable mechanistic insights into how NAD^+ immunometabolic signaling controls astrocyte activation and promotes CNS autoimmunity.

Multiple sclerosis (MS) is a chronic immune-mediated disease of the central nervous system (CNS) that involves both peripherally driven and compartmentalized inflammation within the CNS (1). Although both MS and its animal model, experimental autoimmune encephalomyelitis (EAE), are considered autoimmune disorders, recent data suggest that various metabolic aspects, including the cellular lipid profile and bioenergetic potential, play a critical role in disease progression (2–6). Astrocytes are the most abundant cells in the CNS and perform essential functions during development and homeostasis. These include participating in the maintenance of the blood–brain barrier (BBB), storing and distributing energetic substrates to neurons and supporting the development of neural cells and synaptogenesis (7–9). Astrocytes respond to acute or chronic stimulation with reactive changes that influence the outcome of a variety of neurological disorders, including MS (1,10–12). Accordingly, astrocytes can influence neurotoxicity, modulate the microglial phenotype, regulate the recruitment of inflammatory cells into the CNS, and shape the immunometabolic landscape (2, 3, 11–14). These activities are driven by transcriptional reprogramming and metabolic adaptations whose contextual diversity and regulation are poorly understood.

Nicotinamide adenine dinucleotide (NAD^+) is an essential small molecule in all organisms, where it is a crucial cofactor in energy production and serves as a substrate for NAD^+-dependent enzymes. NAD^+-dependent signaling pathways regulate a broad spectrum of cellular events, including transcription, epigenetic regulation, DNA damage repair, and metabolism (15, 16). As a result, NAD^+ metabolic dependency contributes to a spectrum of diseases, including metabolic pathologies, cancer, aging, and neurodegeneration disorders (15, 16) and features in the regulation of the peripheral immune response (6, 17). Mammalian cells synthesize NAD^+ by three different pathways (15): de novo synthesis from tryptophan via the kynurenine pathway; generation from nicotinic acid through the Preiss–Handler (PH) pathway; or synthesis from nicotinamide

Author contributions: L.S. and L.M. designed research; T.M., D.S., S.Y., A.T., T.C., A.G.-Y., R.P., N.B.-H., and L.M. performed research; T.M., D.S., S.Y., G.Y., A.T., R.P., L.S., and L.M. analyzed data; and L.S. and L.M. wrote the paper.

The authors declare no competing interest.

This article is a PNAS Direct Submission.

[1]T.M. and D.S. contributed equally to this work.

[2]To whom correspondence may be addressed. Email: liormayo@tauex.tau.ac.il.

This article contains supporting information online at http://www.pnas.org/lookup/suppl/doi:10.1073/pnas.2211310119/-/DCSupplemental.

Published August 22, 2022.

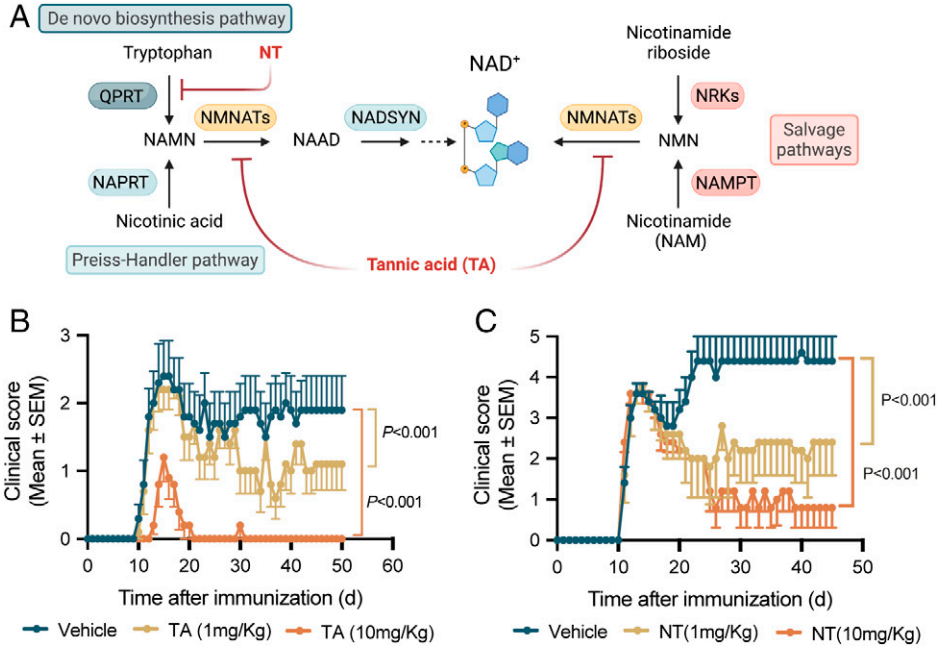

Fig. 1. Inhibition of endogenous NAD$^+$ synthesis ameliorates EAE. (*A*) Overview of NAD$^+$ biosynthetic pathways. Mammalian cells maintain NAD$^+$ levels by three independent pathways (15, 87). First, the de novo synthesis pathway of NAD$^+$ from tryptophan occurs through the kynurenine pathway and results in the synthesis of quinolinic acid, which is transformed into NAMN. At this point, it converges with the Preiss–Handler pathway. Second, the P–H pathway uses dietary nicotinic acid and the enzyme nicotinic acid phosphoribosyltransferase (NAPRT) to generate nicotinic acid mononucleotide (NAMN), which is then transformed into nicotinic acid adenine dinucleotide (NAAD) by NMNATs. Out of the three NMNATs, (the nucleic NMNAT1, cytosolic NMNAT2, and mitochondrial NMNAT3), only NMNAT2 is enriched in the CNS (87). Third, the NAD$^+$ salvage pathway recycles the NAM generated as a by-product of the enzymatic activities of NAD$^+$-consuming enzymes such as CD38. The first step in this pathway is the rate-limiting recycling of NAM by NAMPT, which is then converted into NAD$^+$ via the different NMNATs. TA inhibits NMNAT activity (75), and QPRT activity is inhibited by NT (76). (*B* and *C*) EAE scores (mean and SEM) in mice treated daily, starting 16 d after EAE immunization with (*B*) TA (1 or 10 mg/kg), or (*C*) NT (1 or 10 mg/kg), or vehicle (PBS). n = 10 mice/group, representative of two experiments. Statistical analysis by two-way analysis of variance (ANOVA).

(NAM) or nicotinamide riboside via the salvage pathway (Fig. 1*A*). While systemic NAD$^+$ administration has been reported to attenuate EAE by regulating CD4$^+$ T cell differentiation (6), little is known about the contribution of endogenous NAD$^+$ metabolism to neuroinflammation, especially in the context of the metabolic restrictions enforced by the BBB (9). Thus, we investigated whether perturbation of endogenous NAD$^+$ metabolism regulates astrocyte activation and shapes the neuroinflammatory landscape of CNS autoimmunity.

Here, we report that NAD$^+$, produced by the enzyme nicotinamide phosphoribosyltransferase (NAMPT) of the salvage pathway, drives pathogenic reprogramming of mouse and human astrocytes and promotes neuroinflammation. Concomitantly, we also identified a key role of the NAD$^+$-consuming enzyme CD38 in orchestrating the inflammatory responses of astrocytes that promote the pathogenesis of EAE. The results of our study reveal the NAMPT–CD38 circuitry as a critical factor for regulating astrocyte activation and CNS autoimmunity via the regulation of calcineurin/NFAT signaling, thereby exposing targetable vulnerabilities in the neuroinflammatory signaling cascade, with therapeutic potential for treating MS and other neuroinflammatory disorders.

Results

Inhibition of Cell-Autonomous NAD$^+$ Synthesis Ameliorates EAE. Cellular NAD$^+$ concentrations change during inflammation and aging, and modulation of NAD$^+$ usage or production can control overall health and life span. This has led to the development of different therapeutic strategies for manipulating NAD levels (6, 15, 18). However, little is known about the contribution of cell-autonomous NAD$^+$ synthesis to autoimmune CNS inflammation. To investigate the role of endogenous NAD$^+$ in EAE, we inhibited NAD$^+$ synthesis using the nicotinic acid phosphoribosyl transferase (NMNAT)-specific inhibitor tannic acid (TA) and the quinolinate phosphoribosyl transferase (QPRT) inhibitor, 3-nitropyridine-2-thione as illustrated in Fig. 1*A* (19). The results indicated that daily administration of either TA or 3-nitropyridine 2-thiol (NT) suppresses disease progression in mice in a dose-dependent manner compared to vehicle-treated animals, as determined by the clinical score (Fig. 1 *B* and *C*). Thus, these data suggest that endogenous NAD$^+$ synthesis exacerbates CNS inflammation.

Inflammatory Astrocytes Depend on NAD$^+$ Salvage. Astrocyte NAD$^+$ metabolism regulates neuronal redox state and blood flow, which are essential for the metabolic homeostasis of a healthy brain (19). However, although astrocytes contribute to the pathogenesis of multiple sclerosis and EAE (1), there is little information about the immunometabolic mechanisms that govern astrocyte activities in autoimmune inflammatory demyelinating disease of the CNS, and specifically about the role of their NAD$^+$ metabolism. To investigate the metabolic dependency of reactive astrocytes on NAD$^+$, we used mouse primary astrocyte cultures treated with lipopolysaccharide and interferon-γ (LPS/IFNγ), a potent stimulus that has been linked to neuroinflammation and MS pathology (2). The results revealed significantly elevated NAD$^+$ levels in LPS/IFNγ-activated astrocytes compared to the untreated (control) cells (Fig. 2*A*), suggesting that NAD$^+$ plays a role in the immunometabolic reprogramming of reactive astrocytes. In order to identify the synthesis pathway responsible for this increase in NAD$^+$, we then analyzed the expression of the key enzymes in the de novo, P–H, and salvage pathways (as illustrated in Fig. 1*A*). RNA-sequencing (RNA-seq) analysis of LPS/IFNγ-stimulated astrocytes identified significant up-regulation of *Nampt*, the rate-limiting enzyme of the NAD$^+$ salvage pathway (20) (Fig. 2*B*). This was further validated by qPCR and immunoblotting on independent samples (Fig. 2 *C* and *D*). Moreover, it is in agreement with RNA-seq–based analysis of the NAD$^+$ synthesis pathways on astrocytes isolated from naïve or EAE mice (21), which similarly revealed significant up-regulation only in genes associated with the NAD$^+$ salvage pathway (*Nampt* and *Nmnat2*, *SI Appendix*, Fig. S1*A*). Notably, although the inhibition of the kynurenine pathway ameliorated EAE progression, this pathway was virtually absent in astrocytes (primary cells or astrocytes isolated from naïve or EAE mice) (*SI Appendix*, Fig. S1 *B–D*), in agreement with previous analyses

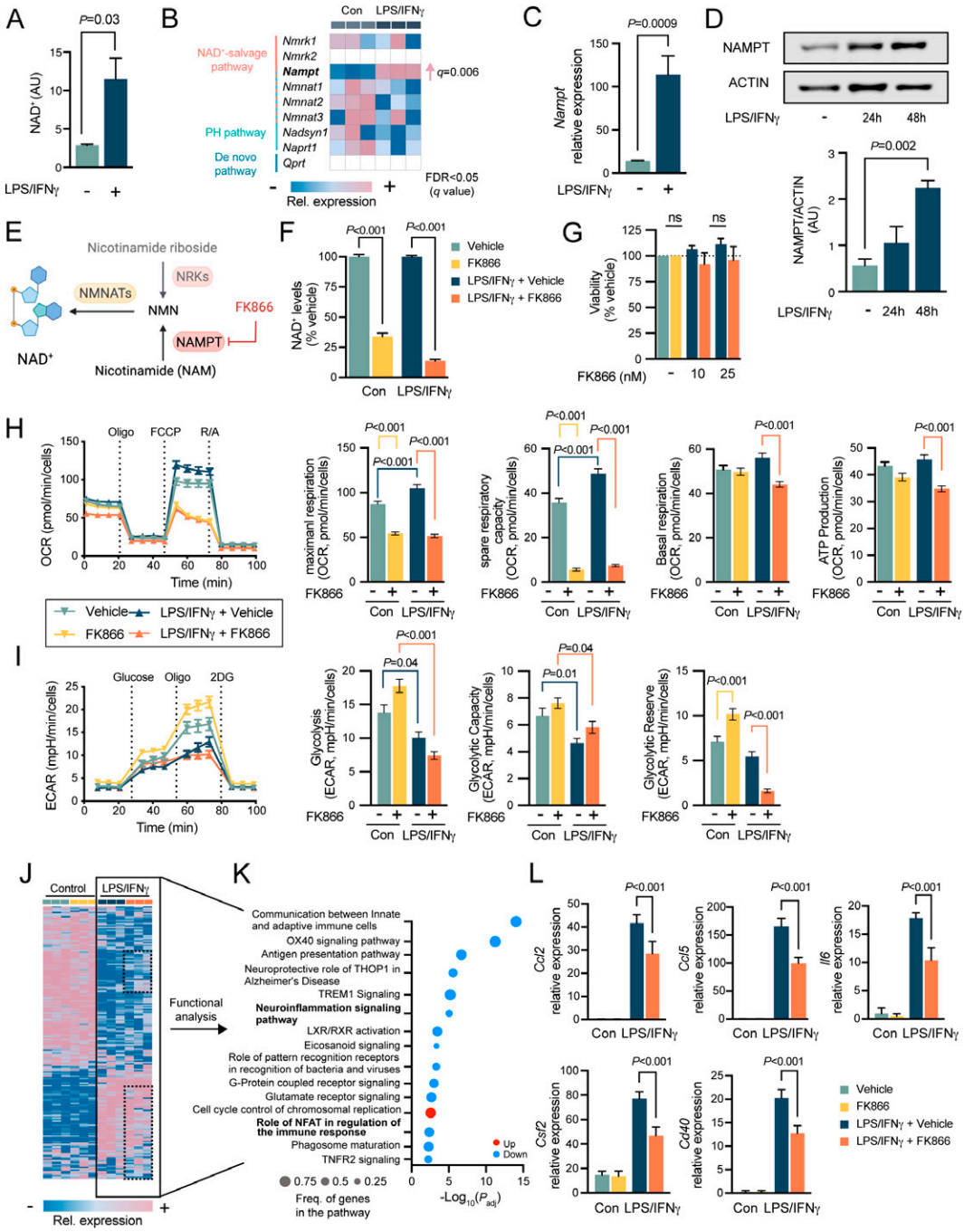

Fig. 2. NAMPT drives the bioenergetic reprogramming of inflammatory astrocytes. Primary astrocytes activated for 6 h (*B*, *C*, *J*, and *L*) or 18 h (*A*, *D*, and *F–I*) with lipopolysaccharide (100 ng/mL) and interferon-γ (100 ng/mL) (LPS/IFNγ) or left untreated (control [Con]); in some experiments, astrocytes were pretreated for 1 h with FK866 (10 nM) or vehicle control (vehicle) (*F–L*). (*A*) NAD^+ levels are quantified by LC-MS/MS, based on the area under the curve ($n = 3$ biologically independent samples, representative of three independent experiments). (*B*) Heatmap comparing the transcriptional expression of key NAD^+ synthesis enzymes; analysis of RNA-seq expression ($n = 3$). Statistical analysis by two-way ANOVA, false discovery rate (FDR) corrected q values for multiple compressions are presented; q values <0.05 were considered statistically significant. CPM, counts per million mapped reads. (*C*) qPCR analysis of *Nampt* expression normalized to *Ppia* ($n = 4$ biologically independent experiments). (*D*) Representative immunoblot and quantification analyses comparing NAMPT protein levels ($n = 3$ biologically independent experiments). (*E*) Schematic representation of the NAMPT inhibition of the NAD^+ salvage pathway by FK866. (*F*) NAD^+ levels in FK866-treated astrocytes, compared to vehicle treatment ($n = 6$, representative of two independent experiments). (*G*) Viability of astrocytes pretreated with FK866 (10 nM or 25 nM) or vehicle and activated with LPS/IFNγ ($n = 3$). (*H* and *I*) Real-time changes in the OCR (*H*) and ECAR (*I*) of astrocytes, pretreated with FK866 (10 nM) or vehicle, then activated with LPS/IFNγ for 18 h and measured using Seahorse. Oligo, oligomycin; FCCP, carbonyl cyanide4-(trifluoromethoxy) phenylhydrazone; R/A, rotenone plus antimycin A; 2-DG, 2-deoxy-d-glucose. basal respiration, spare respiratory capacity, maximal respiration, and ATP production were determined based on OCR readings. Glycolytic reserve, glycolysis, and glycolytic capacity were extracted from ECAR. Data are representative of three independent experiments ($n = 6$ technical replicates per experiment). (*J* and *K*) RNA-seq analysis of astrocytes pretreated with FK866 or vehicle control and activated with LPS/IFNγ. (*J*) Heatmap of differently expressed genes (at least two-fold change, *P*adj < 0.01) and (*K*) IPA canonical pathway analysis presents the activated gene frequency (dot size), intensity (color coded), and *P* value. (*L*) qPCR analysis of neuroinflammatory genes (*Ccl2*, *Ccl5*, *Il6*, *Csf2*, *and Cd40*; expression normalized to *Ppia*, $n = 4$ biologically independent experiments). Data are shown as mean ± SEM. *P* values were determined by two-sided Student's *t* tests (*A* and *C*), one-way ANOVA (*D*), or two-way ANOVA (*F–I*, and *L*) followed by Bonferroni post hoc analysis; *P* values <0.05 were considered statistically significant. Transcriptomic data in *C* and *L* were obtained on independent samples to those used for RNA-seq analysis (*B* and *J*). AU, arbitrarily units.

(22). Conversely, transcriptional analysis of primary glial cells identified that *Qprt* expression is limited to microglial cells (*SI Appendix*, Fig. S1*E*), and is significantly more abundant in microglial cells isolated from naïve or EAE mice compared to astrocytes (*SI Appendix*, Fig. S1*F*). Moreover, in models of neuroinflammation (23, 24) and brain tumors (25), quinolinic acid, the substrate of QPRT, is found in the CNS only in myeloid cells and not astrocytes, thus reinforcing the notion that the cellular source for the QPRT/kynurenine pathway in the inflamed CNS is the myeloid cells and not the astrocytes. Collectively, these data suggest that the NAMPT-driven salvage pathway is the primary NAD^+ synthesis pathway in reactive astrocytes.

The correlation between increased NAMPT expression and elevated NAD^+ levels in inflammatory astrocytes suggests that the NAD^+ salvage pathway is employed to attain the NAD^+ levels required for acquiring and maintaining the reactive astrocyte phenotype. To examine this hypothesis, we analyzed the response of astrocytes to LPS/IFNγ stimulation in the presence of FK866, a specific inhibitor of NAMPT (17), as illustrated in Fig. 2*E*. The results presented in Fig. 2 *F* and *G*, respectively, indicate that treatment with FK866 depletes the levels of NAD^+ in naïve and LPS/IFNγ-treated astrocytes, compared to vehicle-treated cells, without diminishing cell viability. Collectively, these data suggest that inflammatory astrocytes rely on NAMPT to meet the metabolic demand for elevated NAD^+ levels.

NAMPT Drives the Bioenergetic Reprogramming of Inflammatory Astrocytes. Astrocytes utilize both glycolytic and mitochondrial pathways to power the cellular processes required to maintain normal CNS functions (26). Recent suggestions implicate bioenergetic reprogramming in astrocyte responses to injury or disease, both with respect to survival but also with regard to the inflammatory response (27–30). Whereas bioenergetic regulation of immune cell inflammatory responses has been the subject of intense study (17, 31–33), the bioenergetic metabolic reprogramming of inflammatory astrocytes remains poorly understood. We hypothesized that the NAMPT-dependent up-regulation of NAD^+ observed in reactive astrocytes is intended to meet their energy demands and/or drive transcriptional inflammatory reprogramming.

To test this hypothesis, we first investigated the bioenergetic dependency of astrocytes on the NAD^+ salvage pathway. To this end, we studied the effects of NAMPT inhibition on mitochondrial oxidative phosphorylation and glycolysis by monitoring the oxygen consumption or extracellular acidification rates (OCR or ECAR, respectively) during astrocyte activation. Our results indicate that astrocyte stimulation with LPS/IFNγ boosts the bioenergetic metabolism, significantly enhancing the respiration rate and the spare respiratory capacity (SRC, indicative of the adaptation to the demand of a sudden increase in energy) (34), while reducing astrocyte dependency on glycolysis (Fig. 2 *H* and *I*). In addition, we found that the NAMPT inhibitor FK866 suppresses the astrocyte's ability to meet these energetic requirements, as demonstrated by a significant inhibition of mitochondrial oxidative phosphorylation and adenosine triphosphate (ATP) production (Fig. 2 *H* and *I*). Taken in conjunction, these results suggest that the NAD^+ salvage pathway plays a crucial role in supporting the energy demands of reactive astrocytes.

Given the dependency of the inflammatory response on cellular metabolism and the importance of NAMPT for this process, we reasoned that inhibition of the NAD^+ salvage pathway would modulate the reactive astrocyte phenotype. We therefore studied the effects of NAMPT inhibition on astrocyte activation (Fig. 2 *J–L* and *SI Appendix*, Fig. S1 *G–I*). The results revealed that FK866 treatment impairs the transcriptional response of astrocytes to stimulation with LPS/IFNγ (Fig. 2*J*) and significantly attenuates the activation of canonical functional pathways linked to neuroinflammation (Fig. 2*K* and *SI Appendix*, Table S1). Consistent with this analysis, the inhibition of genes associated with astrocyte proinflammatory activation (2) was validated in an independent set of FK866-treated astrocyte samples by qPCR (Fig. 2*L*). Similarly, knockdown of NAMPT expression in primary astrocytes attenuated proinflammatory gene expression induced by LPS/IFNγ (*SI Appendix*, Fig. S1 *G–I*). Collectively, these data suggest that NAD^+ salvage is important for the characteristic metabolic program of reactive astrocytes and promotes the transcriptional responses in astrocytes associated with neuroinflammation.

NAD^+ Degradation by the Glycohydrolase CD38 Drives Astrocyte Activation. The observation of a critical role of NAD^+ salvage in reactive astrocytes prompted us to examine the molecular circuits that lead to the reduction in NAD^+ levels. NAD^+ is depleted by NAD^+-consuming enzymes such as glycohydrolases (CD38 and CD157), poly(ADP ribose) polymerases (PARPs), and sirtuins (SIRTs) (15). To identify the NAD^+-catabolizing enzymes that are physiologically relevant to neuroinflammation, we used RNA-seq data released by van Wageningen et al. (35) to analyze their expression in demyelinated white and gray matter areas of patients with multiple sclerosis. The results revealed that only two NAD^+-degrading enzymes (*CD38* and *PARP14*) were significantly up-regulated in demyelinated lesions (*SI Appendix*, Fig. S2*A*), which is in line with the reported up-regulation of CD38 protein levels in MS lesions (36), and in different mouse models of demyelination (36, 37). Analysis of single-nucleus RNA sequencing (snRNA-seq) studies (35) of *CD38* and *PARP14* expression identified that the expression of *CD38* was significantly more robust than *PARP14* in astrocytes from normal brain tissue and MS plaques (*SI Appendix*, Fig. S2*B*). Next, we analyzed the expression of *Cd38* and *Parp14* in mouse primary cultures (38) and brain and spinal cord astrocytes (39, 40). Similar to the expression patterns in human astrocytes, the results revealed that *Cd38* is expressed mainly by astrocytes in the naïve murine CNS, where it appears at significantly higher levels than *Parp14* (*SI Appendix*, Figs. S2 *C–G*).

To explore astrocyte *CD38* expression during inflammation, we studied two models of neuroinflammation (acute injury and EAE) in which astrocytes are known to play a prominent role (11). scRNA-seq analysis of reactive astrocytes following spinal cord injury (41) identified up-regulation of *Cd38* levels compared to the astrocyte from naïve spinal cord tissue (*SI Appendix*, Fig. S2 *H* and *G*, respectively). Concomitantly, mRNA analysis of astrocytes isolated from acute and chronic models of EAE (2, 42) identified significant up-regulation of *Cd38* during active inflammation (*SI Appendix*, Fig. S2 *I* and *J*). Collectively, these data suggest that CD38 is the main NADase in the CNS in the context of neuroinflammation and that it is expressed mainly in astrocytes. Indeed, CD38 is a major NAD^+-consuming enzyme, and mice lacking (knockout) CD38 ($CD38^{KO}$) show up to a 10-fold increase in brain NAD^+ levels and no brain NADase activity (15, 37, 43). Moreover, in line with previous reports suggesting that targeting CD38 activity regulates models of demyelination (36, 37), we found that CD38 deficiency results in suppression of EAE progression in terms of clinical score, demyelination, and axonal loss (*SI Appendix*, Fig. S3 *A* and *B*) (33, 34). Taken together, these data suggest that CD38 plays an important role in promoting neuroinflammation and support the notion that this enzyme mediates NAD^+ depletion in reactive astrocytes.

To test this hypothesis further, we investigated the effects of CD38 depletion on astrocyte NAD^+ levels and their transcriptional response to activation. As expected, the levels of NAD^+ in CD38-deficient primary astrocytes (Fig. 3*A*) were significantly elevated (3.6 ± 0.54-fold), which is consistent with the in vivo measurements of NAD^+ levels in the CNS of $CD38^{KO}$ mice (37, 43). To study the regulation of astrocyte activation by CD38, we stimulated wild-type (WT) and CD38-deficient primary astrocytes with LPS/IFNγ and analyzed their mRNA expression by RNA-seq (Fig. 3 *B* and *C*). The results revealed 329 differentially regulated transcripts in LPS/IFNγ-stimulated CD38-deficient astrocytes compared to activated WT astrocytes (Fig. 3*B*). Consistent with the observed perturbation of the NAD^+ levels, Ingenuity pathway analysis (IPA) revealed that many of the genes associated with mitochondrial and bioenergetic activity were up-regulated by CD38 ablation. Conversely, activated astrocytes depleted of CD38 have a lower expression of transcripts linked to the regulation of the immune response (e.g., communication between innate and adaptive immune cells and neuroinflammation signaling pathways). This observation was further validated by qPCR in an independent set of astrocyte samples (Fig. 3*D*). Moreover, we have also identified that CD38 deficiency inhibited the signaling cascade associated with key transcription factors, such as NF-κB, IRF, and NFAT. Indeed, we have previously shown (2) that IRF1 and NF-κB promote the reprogramming of pathogenic astrocytes during EAE (Fig. 3*C* and *SI Appendix*, Table S2). Importantly, we found that inhibition of CD38 activity mirrors the regulatory function of CD38 ablation in programming astrocyte pathogenicity. Accordingly, inhibition of CD38 by the specific inhibitor 78C (36) (*SI Appendix*, Fig. S3*C*) suppressed CD38 activity and attenuated the up-regulation of inflammatory genes (*Ccl2*, *Clc5*, *Il6*, *Csf2*, and *Cd40*) in LPS/IFNγ-stimulated WT astrocytes, but not in CD38-deficient cells (*SI Appendix*, Fig. S3 *D* and *E*, respectively). In addition, treatment with the NAD^+ analog β-nicotinamide-8-bromoadenine dinucleotide (8Br-NAD), which, as illustrated in *SI Appendix*, Fig. S3*H*, inhibits CD38-mediated signaling (44), attenuated astrocyte activation (*SI Appendix*, Fig. S3*J*). Moreover, intranasal administration of 8Br-NAD attenuated the clinical course of EAE (*SI Appendix*, Fig. S3*I*) in a manner reminiscent of the effect of CD38 depletion on the disease course (*SI Appendix*, Fig. S3*A*). Notably, intranasal drug administration is highly efficient in circumventing the BBB to deliver therapeutic targets to the CNS (45, 46) and is an effective route to transport NAD^+ to the brain (47–49). Taken together, these data suggest that NAD^+ bioavailability, controlled by the cross-talk between CD38 and NAMPT, regulates astrocyte activation.

We, therefore, reasoned that there should be a functional and molecular correlation between the NAMPT-mediated and CD38-regulated impact on astrocyte activation. To investigate the functional correlation between NAMPT and CD38 regulation on the response of LPS/IFNγ-stimulated astrocytes, we compared the statistical significance of the IPA-identified canonical pathway found to be regulated by the two enzymes (Figs. 2*K* and 3*C*, respectively). The results revealed a significant correlation between the two datasets ($P < 0.0001$, $R^2 = 0.4627$; Fig. 3*E*) and specifically in pathways associated with neuroinflammation and immune regulation (Fig. 3*F*). In accordance with these results, we identified a significant correlation ($P = 0.0009$) between the molecular perturbations induced by NAMPT inhibition or CD38 deficiency of the "neuroinflammation singling pathway" gene signature (Fig. 3*G*), thus suggesting that the NAMPT–CD38 immunometabolic circuit controls astrocyte proinflammatory activation. Consistent with this interpretation, FK866 treatment of LPS/IFNγ-stimulated astrocytes suppressed the activation of the WT cells, as exemplified by the transcriptional analysis of the neuroinflammatory genes *Ccl2*, *Ccl5*, *Il6*, and *Cd40*, but did not affect the expression of these genes in CD38-deficient astrocytes (Fig. 3*H*).

CD38 Activity in Astrocytes Exacerbates CNS Inflammation. Astrocytes are important neuroinflammation regulators in autoimmune CNS inflammation (2, 3, 50, 51). To investigate the role of CD38 signaling in astrocytes during EAE, we knocked down the expression of CD38 using a previously established (2, 3, 42) lentivirus-based system optimized for astrocyte-specific knockdown in vivo (Fig. 3*I*). In this system, the truncated GFAP promoter, GfaABC1D, drives the expression of a miR30-based validated shRNA sequence and a GFP reporter. When a *Cd38*-specific or a nontargeting shRNA encoding lentivirus (*Gfap*-sh*Cd38* and *Gfap*-shNT, respectively) were administered intracerebroventricularly at 7 and 14 d after EAE induction, CD38 expression was efficiently knocked down in astrocytes isolated from G*fap*-sh*Cd38* treated mice, compared to control mice receiving the *Gfap*-shNT lentivirus (Fig. 3*J*). In addition, in agreement with CD38 support of the proinflammatory signature, silencing CD38 expression in reactive astrocytes could ameliorate EAE severity, as indicated by lower disease scores (Fig. 3*K*).

Astrocytes play an important role in the recruitment of inflammatory monocytes into the CNS, which is mainly driven by CCL2 and promotes neurodegeneration and neuroinflammation (52, 53). Our observation that CD38 controls *Ccl2* expression in activated astrocytes (Fig. 3*D* and *SI Appendix*, Fig. S3 *E* and *J*) prompted us to reason that inhibiting CD38 activity would hinder the ability of astrocytes to induce monocyte migration. Indeed, astrocyte conditioned media (ACM) collected from astrocytes that were primed with LPS/IFNγ in the presence of 78C (ACM_{78C}), as illustrated in *SI Appendix*, Fig. S3*F*, was significantly less chemoattractive to inflammatory monocytes than control ACM (ACM_{veh}) (*SI Appendix*, Fig. S3*G*). This suggests that CD38 activity regulates the ability of astrocytes to recruit monocytes to the CNS. We therefore next investigated whether *Cd38* expression in astrocytes could attenuate the recruitment of inflammatory monocytes into the CNS of EAE mice. To this end, we administered the *Gfap*-sh*Cd38* or *Gfap*-shNT lentivirus to EAE mice (as in Fig. 3*K*) and analyzed monocyte recruitment to the CNS by flow cytometry at the peak of the disease. The results indicated that CD38 knockdown in reactive astrocytes significantly reduces the frequency of monocyte (defined as $CD11b^+CD45^{high}$ cells) recruitment to the CNS during EAE (Fig. 3*L*). Hence, these data demonstrate that CD38 activity in astrocytes is detrimental to CNS inflammation.

NFAT Signaling Mediates the CD38 Regulation of Proinflammatory Astrocytes. We next attempted to identify the molecular mechanism underlying the inflammatory phenotype associated with CD38 activity in astrocytes. CD38 hydrolysis of NAD^+ generates nicotinamide, cyclic adenosine diphosphate (ADP) ribose (cADPR), and ADPR (as illustrated in *SI Appendix*, Fig. S3*C*) (54). While nicotinamide drives the NAMPT-dependent NAD^+ salvage pathway, cADPR and ADPR are putative second messengers that induce calcium release from the endoplasmic reticulum, or elicit Ca^{2+} influx across the plasma membrane, respectively. Both these effects modulate the activation of immune cells (44, 55–57). Indeed, mass spectrometry analysis of cADPR and ADPR levels in naïve and activated astrocytes detected a significant increase in the levels of the two metabolites following LPS/IFNγ stimulation (Fig. 4 *A* and *B*). Importantly, the accumulation of

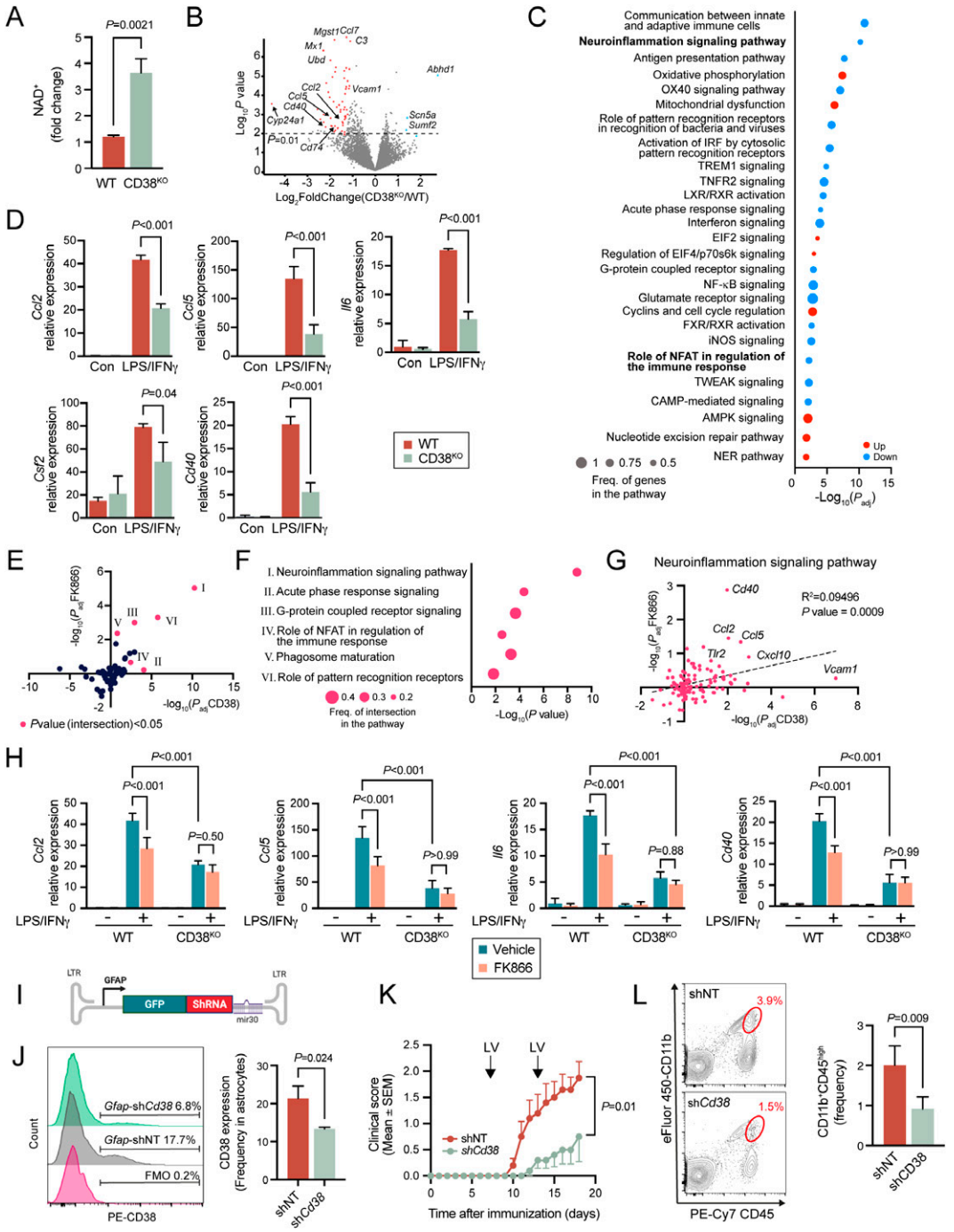

Fig. 3. CD38 activity promotes astrocyte activation and pathogenesis of EAE. (*A*) NAD^+ levels were quantified by LC-MS/MS. ($n = 3$ biologically independent samples, representative of three independent experiments). (*B–D*) Primary WT or CD38 deficient ($CD38^{KO}$) astrocytes activated for 6 h with LPS/IFNγ or left untreated (Con). (*B*) Volcano plot comparing gene expression between LPS/IFNγ-treated WT and $CD38^{KO}$ astrocytes; analysis of RNA-seq expression ($n = 3$). (*C*) IPA canonical pathway analysis presenting the activated gene frequency (dot size), intensity (color coded), and *P* value. (*D*) qPCR analysis of neuroinflammatory genes (*Ccl2*, *Ccl5*, *Il6*, *Csf2*, *and Cd40*; expression normalized to *Ppia*, $n = 3$ biologically independent experiments). (*E* and *F*) Hypergeometric distribution of differently regulated IPA canonical pathways of FK866-treated and CD38-deficient LPS/IFNγ-stimulated astrocytes; pathways with significant intersection ($P < 0.05$) in pink. (*F*) Analysis of the top five enriched pathways presents the intersection frequency (dot size) and *P* values for a hypergeometric enrichment test. (*G*) Hypergeometric distribution of differently regulated genes in the neuroinflammation signaling pathway of FK866-treated and CD38-deficient LPS/IFNγ-stimulated astrocytes; statistics by Pearson correlation (R^2, two tailed). (*H*) Primary WT or $CD38^{KO}$ astrocytes, pretreated with FK866 or vehicle (as in Fig. 2), then stimulated for 6 h with LPS/IFNγ or left untreated (Con); qPCR analysis of neuroinflammatory genes (*Ccl2*, *Ccl5*, *Il6*, *and Cd40*; expression normalized to *Ppia*, $n = 3$ biologically independent experiments). (*I* and *J*) Intracerebroventricular injection of astrocyte-specific sh*Cd38* lentivirus ameliorates disease severity. WT mice were injected intracerebroventricularly with 1×10^7 IU of shNT or sh*Cd38* lentivirus on days 7 and 14 after EAE induction. ($n = 10$ mice per group; representative data of three independent experiments). (*I*) Schematic map of the astrocyte-specific shRNA lentiviral vector. (*J*) Representative flow cytometry plots of CD38 staining in astrocyte-enriched cells from each group are shown on the *Left*, and quantification analyses are on the *Right*. (*K*) EAE scores (mean and SEM). (*L*) Representative flow cytometry plots (*Left*) and quantification analyses of the frequency of $CD11b^+$ $CD45^{high}$ monocytes (*Right*), as determined in the CNS 7 d after the final injection of astrocytes-specific shRNA lentivirus. Data are shown as mean ± SEM. *P* values were determined by two-sided Student's *t* tests (*A*, *J*, and *L*), one-way ANOVA (*D*), or two-way ANOVA (*D*, *E*, and *K*) followed by Bonferroni post hoc analysis (*D* and *E*); *P* values <0.05 were considered statistically significant.

these metabolites was CD38 dependent, as ablation of CD38 significantly reduced their levels (Fig. 4 *C* and *D*). Therefore, we investigated whether using the cell-permeable antagonists 8-Bromo-cADPR (8Br-cADPR) or 8Br-ADPR inhibits cADPR or ADPR signaling (as illustrated in Fig. 4*E*) would regulate astrocyte activation. In agreement with the attenuation of astrocyte activation by the CD38 inhibitors 78C and 8Br-NAD (*SI Appendix*, Fig. S3 *E* and *J*), inhibition of cADPR or ADPR signaling decreased the expression of the proinflammatory-encoding genes *Ccl2*, *Ccl5*, *Ccl7*, *Il6*, and *Cd40* in LPS/IFNγ-treated astrocytes (Fig. 4*F*). These data support the view that CD38 signaling, mediated by cADPR and ADPR, controls astrocyte proinflammatory transcriptional reprogramming.

Interestingly, our perturbations of the NAMPT–NAD^+–CD38 circuitry in activated astrocytes also affected the "role of NFAT in the regulation of the immune response" pathway (Figs. 2*K* and 3 *C* and *F*, and *SI Appendix*, Fig. S4*A* and Tables S1 and S2). IPA-independent transcriptional regulator enrichment analysis (58) revealed a significant enrichment in NFAT binding sites in the NAMPT/CD38-regulated genes (55) (*SI Appendix*, Table S3). The nuclear factor of activated T cells (NFAT) transcription factor family plays an important role in regulating adaptive and innate immune responses, including those of astrocytes (50, 59, 60). Since four of the five NFAT family members: NFATC1, NFATC2, NFAC3, and NFATC4 (60) are regulated by Ca^{2+} levels via the activity of the phosphatase calcineurin, we hypothesized that CD38 control of astrocyte activation could be achieved by its generation of the calcium-mobilizing messengers cADPR and ADPR that would result in calcineurin/NFAT signaling. To examine this hypothesis, we first studied the expression of the four Ca^{2+}-dependent NFATs in astrocytes. The results revealed that *Nfatc3* is the most prominent transcript expressed in nonstimulated (control) or LPS/IFNγ-activated primary mouse astrocytes (Fig. 4*G*, $P < 0.001$) and in astrocytes isolated from the CNS of naïve or EAE mice (21) (Fig. 4*H*, $P < 0.002$). Similarly, *NFATC3* is the most abundant transcript in cultured human mature astrocytes (61) (*SI Appendix*, Fig. S4*B*, $P < 0.001$) or in snRNA-seq analysis of astrocytes from control human brain tissue or MS lesions (62) (*SI Appendix*, Fig. S4*C*, $P < 0.001$). These results suggest that NFATC3 is the main NFAT activated in inflammatory astrocytes.

We therefore reasoned that NFATC3 signaling in response to LPS/IFNγ stimulation might account for the CD38-mediated transcriptional reprogramming of the reactive astrocytes. Accordingly, there was a significant transient accumulation of NFATC3 in the nucleus of WT astrocytes 1 h following LPS/IFNγ-stimulation, which did not occur in the absence of CD38 expression ($P = 0.03$ or 0.98, respectively) (Fig. 4*I*). This was further investigated using the potent and selective NFAT inhibitor INCA-6, which prevents NFAT dephosphorylation and consequent activation by calcineurin (as illustrated in *SI Appendix*, Fig. S5) (63). INCA-6 treatment led to significant attenuation in the induction of neuroinflammatory genes (*Ccl2*, *Ccl5*, *Ccl7*, *Cxcl10*, and *Cd40*) (Fig. 4*J*). Importantly, inhibition of NFAT signaling did not affect the levels of these genes in the absence of CD38 expression. In addition, INCA-6 inhibition attenuated the astrocyte chemotactic potential, similarly to the observed effect of inhibiting CD38 (*SI Appendix*, Fig. S3*G*). Accordingly, ACM, generated following inhibition of NFAT signaling (ACM_{INCA-6}) as illustrated in Fig. 4*K*, was significantly less chemoattractive to inflammatory monocytes than control ACM (ACM_{veh}) (Fig. 4*L*). Taken together, these data suggest that NFAT signaling is responsible for the CD38-mediated transcriptional reprogramming in inflammatory astrocytes.

NAMPT–CD38–NFAT Circuitry Promotes the Proinflammatory Response of Primary Human Astrocytes. To evaluate the functional relevance for human disease, we next studied whether perturbation of the NAMPT–CD38–NFAT circuitry also modulates the activity of human astrocytes. To this end, human primary astrocytes were activated by LPS/IFNγ in the presence of FK866, 78C, INCA-6, or appropriate vehicle control. The results indicated that inhibition of NAMPT, CD38, or calcineurin/NFAT signaling (Fig. 5 *A*–*C*, respectively) leads to a significant decrease in the induction of *CCL2*, *CCL5*, *CCL7*, *IL6*, and *CSF2*. Thus, our findings reveal the NAMPT–CD38–NFAT circuitry as a potential therapeutic target for the regulation of astrocyte activity in human neuroinflammatory disorders.

Discussion

Astrocyte dysfunction is present in numerous diseases, including multiple sclerosis, Alzheimer's disease (AD), Parkinson's disease, and brain tumors (11). A better understanding of the mechanisms that govern astrocyte pathogenicity is required to identify new therapeutic approaches for neurological disorders. However, little is known about immunometabolic circuits that control astrocyte activity. NAD^+ metabolism is involved in many biological processes, and its dysregulation controls the peripheral immune response (6, 17) and has been associated with various pathologies ranging from cancer to neurodegeneration (15, 16, 20). However, the role of NAD^+ metabolism in regulating reactive astrocytes remains elusive. Here we explored the underlying basis and functional significance of NAD^+ metabolism in astrocytes stimulated with LPS/IFNγ or in autoimmune CNS inflammation and validated the physiological relevance of our findings in human astrocytes and MS patients. Our data indicate that astrocyte NAD^+ metabolism, balanced between its synthesis via the NAD^+ salvage pathway and degradation by the glycohydrolase CD38, controls the inflammatory responses of astrocytes. Taken together, the results of our study describe a mechanism by which the CD38 signaling cascade impacts calcineurin/NFAT signaling to promote the proinflammatory transitional reprogramming of reactive astrocytes.

We show elevated levels of NAD^+ in the reactive astrocytes, which could be attributed to the engagement of the NAD^+ salvage pathway since *Nampt* was the only one of the rate-limiting enzymes in the different NAD synthesis pathways to be significantly up-regulated in reactive astrocytes. In line with previous reports demonstrating that astrocyte response to injury or disease is associated with their bioenergetic reprogramming (27–30), we could demonstrate that astrocyte oxidative phosphorylation capacity is linked to their proinflammatory polarization. Thus, if the NAD^+ salvage pathway is functioning to maintain NAD^+ pools, we would expect that inhibiting this pathway would lead to diminished mitochondrial activity. Consistent with this idea, we found that NAMPT inhibition dramatically hampered cell respiration and attenuated ATP production. Interestingly, while both LPS/IFNγ-activated astrocytes and macrophages rely on NAD^+ salvage to maintain their energetic demands, astrocytes favor the oxidative phosphorylation pathway, whereas macrophages depend heavily on glycolysis and Warburg metabolism (17). This represents a distinct metabolic difference between the two cell types that often interact closely during CNS inflammation and opens the possibility for differential regulation of their activity in disease. Consistent with the importance of NAD^+ availability for the differentiation of peripheral immune cells (6, 17) and the reported effects of NAMPT inhibition on cytokine production by macrophages (17), NAMPT inhibition or

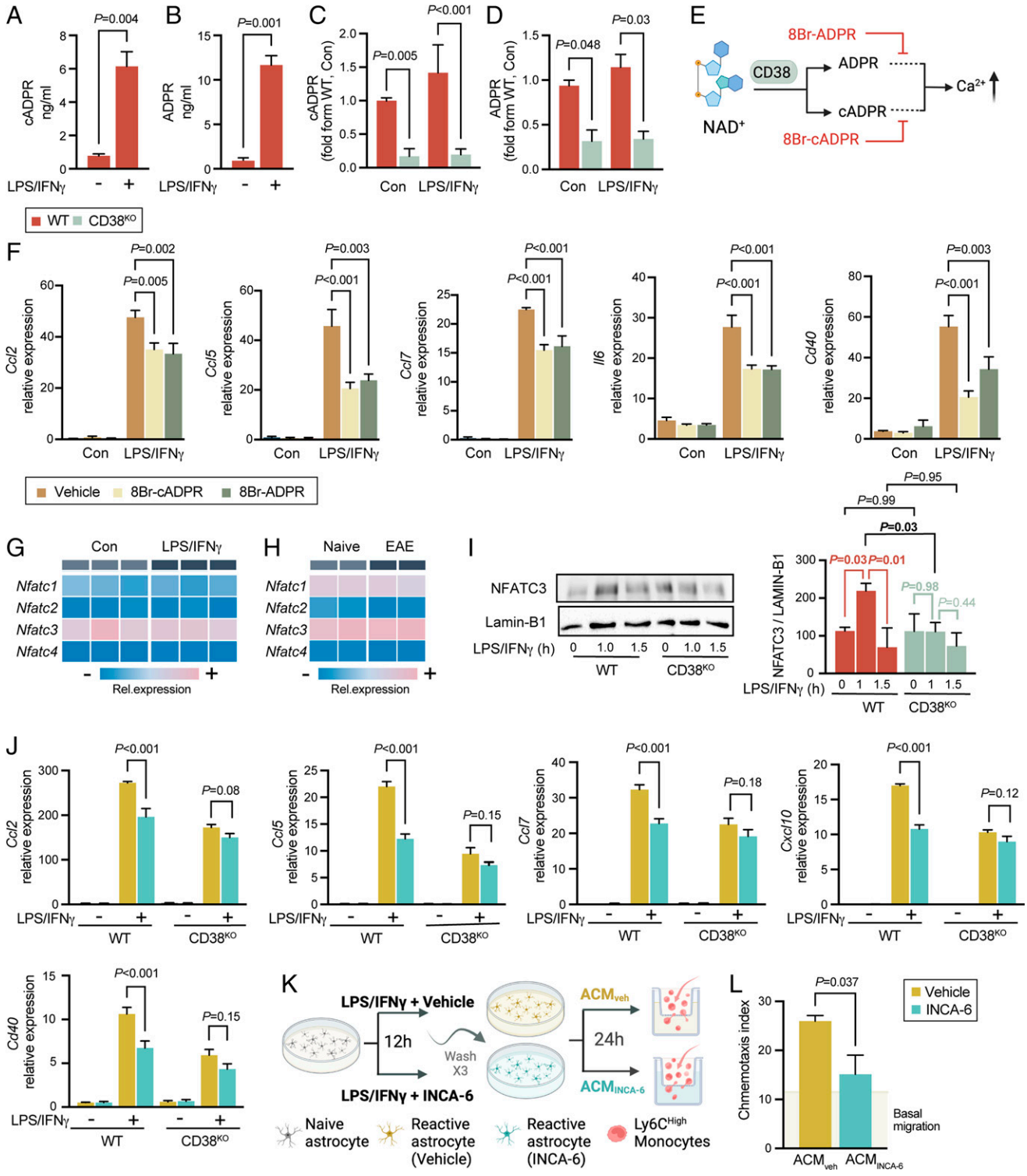

Fig. 4. NFAT signaling mediates the CD38 regulation of proinflammatory astrocytes. (*A*–*D*) cADPR and ADPR levels are quantified by LC-MS/MS in WT and CD38^{KO} astrocytes activated with LPS/IFNγ for 6 h. (n = 3 biologically independent samples, representative of three independent experiments). (*E*) illustration of 8Br-cADPR and 8Br-ADPR mode of action. (*F*) qPCR analysis of neuroinflammatory genes (*Ccl2*, *Ccl5*, *Ccl7*, *Il6*, and *Cd40*; expression normalized to *Ppia*) in cultured astrocytes, pretreated with 200 μM 8Br-cADPR, 8Br-ADPR, or vehicle control, and activated with LPS/IFNγ, 6 h following LPS/IFNγ induction. (n = 4 biologically independent experiments). (*G* and *H*) Expression of *Nfatc1*, *Nfatc2*, *Nfatc3*, and *Nfatc4* in mouse astrocytes. (*G*) mRNA expression in cultured astrocytes; RNA-seq data as in Fig. 3*B*. (*H*) Astrocytes isolated from naïve or EAE mice; RNA-seq data from Rothhammer et al. (21). (*I*) Representative immunoblot (*Left*) of NFATC3 and Lamin B1 expression in nuclear fractions of WT and CD38^{KO} astrocytes activated with LPS/IFNγ for 1 or 1.5 h or left untreated. The degree of NFATC3 translocation to the nucleus was assessed by the ratio between the expression of NFATC3 and Lamin B1 in the nuclear fractions following densitometric quantification on three independent experiments (*Right*). (*J*) Primary WT or CD38^{KO} astrocytes, pretreated with INCA-6 (15 μM) or vehicle, then stimulated for 6 h with LPS/IFNγ or left untreated (Con); qPCR analysis of neuroinflammatory genes (*Ccl2*, *Ccl5*, *Ccl7*, *Cxcl10*, *and Cd40*; expression normalized to *Ppia*, n = 3 biologically independent experiments). (*K* and *L*) Inhibition of astrocyte calcineurin/NFAT signaling attenuates their ability to recruit Ly6C^{high} inflammatory monocytes. Astrocytes were pretreated with INCA-6 or vehicle, followed by activation with LPS/IFNγ for 12 h, then washed extensively and used to prepare astrocyte conditioned medium (ACM$_{INCA-6}$ and ACM$_{veh}$, respectively; as illustrated in *K*), which was tested in an in vitro monocyte migration assay (*L*). Data are shown as mean ± SEM. *P* values were determined by two-sided Student's *t* tests (*A*, *B*, and *L*), one-way ANOVA (*F*), or two-way ANOVA followed by Bonferroni post hoc analysis (*C*, *D*, *I*, and *J*); *P* values <0.05 were considered statistically significant.

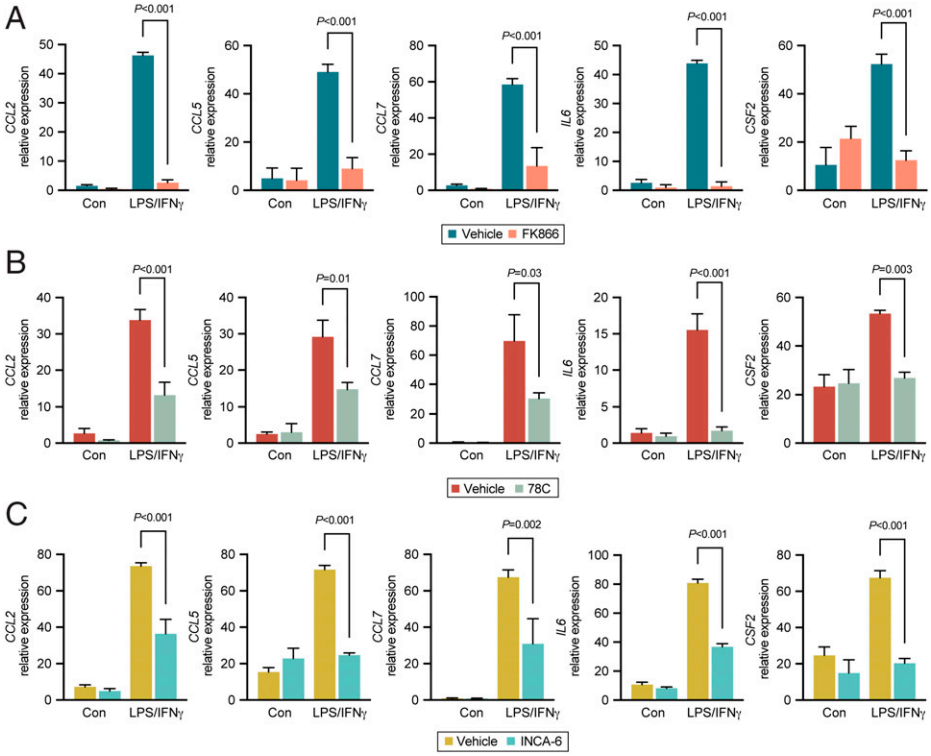

Fig. 5. Inhibition of NAMPT, CD38, or calcineurin/NFAT signaling attenuates primary human astrocyte activation. Primary human astrocytes were pretreated with FK866 (2 μM) (*A*), 78C (8 μM) (*B*), INCA-6 (15 μM) (*C*), or vehicle, and activated with LPS/IFNγ or left untreated (Con). RNA was harvested 6 h later, and the expression of *CCL2*, *CCL5*, *CCL7*, *IL6*, and *CSF2* was analyzed by qPCR relative to *PPIA* in three independent experiments. *P* values were determined by two-way ANOVA followed by Bonferroni post hoc analysis. *P* values <0.05 were considered statistically significant.

knockdown attenuated astrocyte induction of neuroinflammatory pathways. These data suggest that NAD^+ salvage is a crucial pathway in inflammatory astrocytes and supports their metabolic bioenergetic demands and transcriptional reprogramming.

As we sought to understand events leading to NAD^+ salvage dependence, we investigated the expression of the NAD-consuming enzymes in lesions and reactive astrocytes in MS patients and mouse astrocytes isolated from the CNS before or after injury or autoimmune inflammation. Our results indicate that CD38 is the main NADase expressed in astrocytes and has a significant association with astrocyte neuroinflammatory activation. We explored the role of the NADase CD38 in astrocyte NAD metabolism and inflammation. We demonstrate that CD38 is directly involved in the process that mediates NAD^+ decline and limits the astrocyte transcriptional responses that promote their proinflammatory activation, inflammatory monocyte recruitment, and the pathogenesis of EAE.

Our current studies further provide evidence that CD38 control of astrocyte activation is mediated via calcineurin/NFAT signaling, specifically NFATC3, engaged by CD38-dependent generation of the Ca^{2+}-mobilizing agents cADPR and ADPR (summarized in *SI Appendix*, Fig. S5). Indeed, hyperactivation of the astrocyte calcineurin/NFAT signaling pathway is associated with CNS injury and models of neurological diseases (36, 64). Accordingly, NFAT signaling in astrocytes was found to depend on CD38 activity in spinal cord demyelination, and the blocking of astrocyte calcineurin/NFATC3 signaling ameliorated AD symptoms in preclinical models (36, 64). However, since CD38 regulates both cellular and extracellular NAD^+ levels, we cannot exclude the possibility that the effect of astrocyte CD38 activity on EAE pathogenicity may also be mediated by elevating extracellular NAD^+ levels that can support the generation of regulatory T cells (6).

Despite significant advances, there are major challenges in treating MS, especially regarding the minimal therapeutic response of progressive MS patients to treatment and the low availability of FDA-approved drugs that target the compartmentalized immune response in the CNS involving the microglial cells and astrocytes, which is considered to drive secondary progressive MS (SPMS) progression (1, 65). Our study identifies the astrocyte NAMPT–CD38–NFAT circuitry as crucial for promoting neuroinflammation via regulation of NAD^+ bioavailability, astrocyte bioenergetic potential, and their transcriptional reprogramming, thereby identifying targetable vulnerabilities in the mechanisms underlying CNS autoimmunity and MS. The mechanisms driving the pathophysiology of progression in MS, both in primary progressive MS (PPMS) and in the transition from relapsing-remitting MS (RRMS) to its progressive form (SPMS), are not well understood. However, several factors, such as patient current age and weight, were shown to increase the risk of progressing to SPMS (1, 65). Interestingly, CD38 dictates age- and weight-related decline in NAD^+ pools (63, 64), and inhibition of CD38 activity in a chronic high-fat consumption model associated with demyelination reduced astrocyte proinflammatory phenotype and improved myelin regeneration. In addition, we recently found a significant ($20 \pm 4.9\%$; $P = 0.044$, by Mann–Whitney test) up-regulation of *NAMPT* levels in astrocytes of progressive MS patients (62). Taken together, these findings suggest that targeting the NAMPT–NAD^+–CD38 pathway could indeed have therapeutic potential for treating MS, including its progressive form. Of note, this notion is further supported by recent discoveries that teriflunomide (Aubagio), an FDA-approved drug for treating RRMS patients, was recently reported to modulate Ca^{2+} levels and cellular respiration in the brain (66) and diminish the ability of primary astrocytes to induce oxidative metabolism to support their inflammatory response (30), which is reminiscent of our proposed mode of action of the NAMPT–CD38 circuitry. Unfortunately, oral administration of teriflunomide did not affect the course of progressive disease (67), which may be due to the patients' characteristically lowered BBB permeability (68). Notably, the clinical need for developing CNS-targeting inhibitors of the NAMPT–CD38

circuitry is not limited only to CNS autoimmunity. It is shared by various neuropathologies ranging from acute trauma to brain malignancies and neurodegenerative disorders (15, 27, 69–71).

The supplement of NAD^+, or its precursors, has been suggested to be of therapeutic value. However, the clinical development of such drugs has been hampered by significant adverse events following systemic administration (71), highlighting the clinical need for brain-specific or astrocyte-targeting routes for drug delivery. Promising approaches could involve the local release of inhibitors, the use of bispecific antibodies to inhibit the enzymatic activity of specific cells, or the use of the intranasal route, which may serve as a unique delivery route to the brain and is now advancing into the clinic (e.g., the nasal N-methyl-D-aspartate (NMDA) receptor antagonist Spravato). Indeed, Li et al., recently reported that the release of a NAMPT inhibitor from brain-implanted microparticles attenuated the progression of primary brain tumors and enhanced their response to immunotherapy (71). Other options are the specific nanobodies recently developed by Baum et al. that inhibit CD38 activity (72) as well as intranasal delivery of NAD (47–49), or the CD38 inhibitor, 8Br-NAD (*SI Appendix*, Fig. S3*G*), which were shown to be beneficial for brain pathologies associated with MS. Importantly, careful consideration should be given to NAD^+ supplementation during CNS neuroinflammation, as elevated NAD^+ could both support recovery and improve the cell bioenergetics, but also boost CD38-mediated pathogenic pathways. In this regard, nicotinamide supplement is of interest, as it will not only be taken by NAMPT to generate NAD^+, but it also has an inherit ability to inhibit CD38 activity. Consistent with this notion, nicotinamide administration was shown to increase spinal cord NAD^+ levels, reduce cell infiltration to the CNS, halt demyelination and axonal loss, and ameliorate the clinical course of EAE (73). However, additional clinical and preclinical studies are required to address this unmet clinical need.

Taken together, our results demonstrate that the dynamics of astrocyte NAD^+ metabolism, balanced by its synthesis via the salvage pathway and degradation by the NADase CD38, controls a broad array of processes that drive astrocyte activation and CNS inflammation. Thus, the modulation of the NAMPT–CD38–NFAT circuitry has promising therapeutic potential for use in MS and other neurologic disorders, in which astrocyte activation contributes to disease pathology.

Materials and Methods

Animals. SJL/J (strain #000686), C57BL/6J (strain #000664), CD38 knockout ($CD38^{KO}$ mice, and B6.129P2-*Cd38*^{tm1Lnd}/J; strain #003727) mice were purchased from The Jackson Laboratory. The mice were housed in recyclable, individually ventilated cages, with a 12-h light/dark cycle, at a temperature of 21 °C, with 50% humidity, and with ad libitum access to water and food. All animal experiments were performed in accordance with state and federal guidelines and regulations and approved by the Stanford or Tel Aviv University institutional animal care and use committees.

Mouse Immunization, EAE, and Histology. EAE was induced in SJL/J mice by subcutaneous immunization with $PLP_{AA139–151}$ (100 μg per mouse) in 100 μL of incomplete Freund's adjuvant, supplemented with 200 μg *Mycobacterium tuberculosis* (strain H37Ra, BD Difco Laboratories #231141). In contrast, 100 μg of $MOG_{AA35-55}$ in 200 μL of complete Freund's adjuvant containing 4 mg/mL H37Ra *M. tuberculosis* was used for C57BL/6J and $CD38^{KO}$ mice, followed by the administration of pertussis toxin (200 ng per mouse; List Biological Laboratories, Inc.) on days 0 and 2 as described previously (2, 74). Mice were weighed daily, and disease severity was assessed in a blinded manner according to a five-point standard scoring system: 0, no clinical signs; 1, loss of tail tone; 2, hindlimb weakness; 3, complete hindlimb paralysis; 4, hindlimb and forelimb paralysis; and 5, moribund or dead. In some experiments, mice were treated with daily administrations of TA, which is a specific NMNAT inhibitor (75), the CD38 inhibitor 8Br-NAD (44) (Biolog #N017), the specific QPRT inhibitor NT (76) (Sigma-Aldrich, #724793), or vehicle control (vehicle). TA (1 mg/kg or 10 mg/kg) was injected subcutaneously, and 8Br-NAD (10 mg/kg) was administered intranasally (47). For histopathology analysis, animals were perfused with Phosphate-buffered saline (PBS), followed by 4% paraformaldehyde in 0.1 M PBS. Paraffin-embedded sections were stained with Luxol Fast Blue for myelin and Bielschowsky silver impregnation for axons as described previously (2, 42).

Primary Astrocyte Cultures. Primary murine astrocyte cultures were prepared as we described previously (2), with minor modifications. Cerebral cortices from 1- to 3-d-old neonatal mice were dissected, carefully stripped of their meninges, and digested with 0.25% trypsin to obtain single cells. The cell suspension was then cultured at 37 °C in humidified 5% CO_2–95% air. The medium was replaced every 4 to 5 d until the mixed glial cultures reached full confluence (10 to 12 d). The cells were then incubated for 72 h with 6 μg/mL clodrosome (Encapsula Nano Sciences LLC, #CLD-8909) to deplete the microglial cells. After this time, the astrocyte monolayer was separated using mild trypsinization (mild T/E) (77), and the resultant single-cell suspension of astrocytes was plated on poly-L-lysine (0.01 mg/mL; Sigma-Aldrich, #P6282)-coated plates. Primary astrocyte cultures were found to be >99% $GFAP^+$ positive by immunofluorescent staining or >99% $GLAST^+$ by Fluorescence-activated cell sorting (FACS) staining, with less than 1% microglial cells ($IBA\text{-}1^+$ or $CD11b^+$ cells, respectively), as previously shown (12) undefined. Primary human astrocytes (ScienceCell, #1800) were grown according to the manufacturer's instructions. In some experiments, cells were pretreated for 2 h with FK866 (Cayman Chemical Company, #13287), 78C (EMD Millipore, #5.38763.0001), NFAT activation inhibitor III (INCA-6; Cayman Chemical Company #21812), 8Br-ADPR (Biolog #B051) 8Br-cADPR (Biolog #B065), 8Br-NAD, or appropriate vehicle control (vehicle; dimethyl sulfoxide (DMSO) or PBS). The astrocytes were activated with ultrapure lipopolysaccharide from *Escherichia coli* K12 strain (100 ng/mL; InvivoGen, #tlrl-peklps) and the appropriate recombinant interferon-γ (100 ng/mL; R&D Systems, #485-IF-100 for mouse astrocytes or #285-IF-100 for human cells, LPS/IFNγ), or left untreated (control).

Metabolic Assays. Metabolite quantitation of primary astrocyte cultures was performed with liquid chromatography coupled to tandem mass spectrometry (LC-MS/MS). To quantify NAD, ADPR, and cADPR, astrocytes were washed twice with ice-cold PBS, and metabolites were extracted with methanol (80%), as described previously (78). LC-MS measurements were performed using an Acquity UPLC I-Class system (Waters), and a Xevo TQ-S triple quadrupole mass spectrometer (Waters) equipped with an electrospray ion source operated in positive ion mode was used for analysis. MassLynx and TargetLynx software (v.4.2, Waters) were applied for data acquisition and analysis. NAD^+ abundance was also measured using the NAD-Glo assay (Promega, #G9071) according to the manufacturer's instructions.

Real-time ECAR and OCR measurements were made with an XF-96 Extracellular Flux Analyzer (Seahorse Bioscience). A total of 1×10^5 cells were plated into each well of Seahorse ×96 cell culture microplates and preincubated at 37 °C for 24 h in 5% CO_2. The sensor cartridge for the Xfe96 analyzer was hydrated in a 37 °C non-CO_2 incubator a day before the experiment. OCR and ECAR were measured under basal conditions and after the addition of the following compounds: 1.5 μM oligomycin, 2 μM FCCP [carbonyl cyanide4-(trifluoromethoxy) phenylhydrazone], 0.5 μM rotenone and 0.5 μM antimycin, 10 mM glucose, and 50 mM 2-deoxy-D-glucose (all obtained from Sigma) as indicated. Data were expressed as the oxygen consumption rate in pmol/min or the rate of extracellular acidification in mpH/min, normalized to the Hoechst 33342 DNA staining in individual wells. Results were processed with Wave software version 2.4 (Agilent).

RNA Interference Experiments. The pLenti-GFAP-EGFP-mir30-shRNA vector backbone (2) in which the truncated GFAP promoter, GfaABC1D, drives the expression of a miR30-based shRNA and a GFP reporter, was used in all RNAI interference (RNAi) experiments. pLenti-GFAP-EGFP-mir30-sh*Nampt* and pLenti-GFAP-EGFP-mir30-sh*Cd38* harboring previously validated shRNA sequences against *Nampt* (TRCN0000101279) (17) or *Cd38* (TRCN0000068230) (79) were cloned into the pLenti-GFAP-EGFP-mir30-sh*B4galt6* vector backbone (2), as we

have described previously (2). The construction of the nontargeting shRNA vector (pLenti-GFAP-EGFP-mir30-shNT) was as previously described (2). Lentivirus particles were then generated by transfecting 3.9×10^6 293T cells using 1.5 μg PEI MAX (Polysciences, #24765-1) with 6.1 μg pLenti-GFAP-EGFP-mir30-shRNA or pLenti-GFAP-EGFP-mir30-shNT vectors with packing plasmids [4.5 μg psPAX2 (Addgene, #12260) and 1.5 μg pMD2.G (Addgene, #12259)]. The supernatant collected 24 h after transfection was concentrated using a Lenti-X Concentrator (Takara, #631232) and stored at −80 °C until use. The viral titer was determined using the qPCR Lentivirus titration kit (ABM, #LV900) according to the manufacturer's instructions.

Primary astrocyte cultures were transduced with sh*Nampt* or shNT viruses (multiplicity of infection [MOI] of 10) for 12 h in the presence of polybrene (8 mg/mL; Sigma Aldrich #H9268). The cells were then washed and allowed to recover for 72 h before NAMPT expression was validated by immunoblotting, or cells were stimulated with LPS/IFNγ.

For in vivo intracerebroventricular injection, mice were anesthetized and positioned in a stereotaxic alignment system. A Hamilton syringe was used to inject sh*Cd38* or shNT viruses (1×10^7 IU/mouse) at a position 0.44 mm posterior and 1.0 mm lateral to the bregma and 2.2 mm below the skull surface. The injection speed was maintained at 1 μL/min to prevent leaking, as we described previously (2).

Chemotaxis Assay. Spleen monocytes ($CD11b^+/CD3^-/CD45R^-/CD117^-/Ly\text{-}6G^-/NK1.1^-/Siglec\ F^-/SSC^{low}$) were isolated from C57BL/6 mice using the EasySep Mouse Monocyte Isolation Kit (Stemcell, #19861). Monocytes were stained with CellTrace CFSE Cell Proliferation (Thermo Fisher Scientific, #C34554), and a total of 2×10^3 monocytes/per well were plated in an IncuCyte ClearView 96-well cell migration plate (Sartorius, #4582), which was precoated with 50 μg/mL Matrigel (Corning, #FAL356237). ACM or control media were added to the lower chamber, and monocyte migration to the lower chamber was measured with an IncuCyte ZOOM system (v2020C) following a 2-h incubation at 37 °C. The chemotaxis index was defined as the percentage of monocytes that infiltrated the lower chamber. To generate ACM, 5×10^6 primary astrocytes were cultivated in a 10-cm culture plate and stimulated for 12 h with LPS/IFNg. In some experiments, astrocytes were also treated with 78C, INCA-6, or vehicle control (vehicle). Media were removed, and the astrocytes were thoroughly washed three times and incubated for 24 h with 8 mL of chemotaxis medium [Dulbecco's Modified Eagle Medium (DMEM) supplemented with 10 mM Hepes and 0.5% bovine serum albumin (BSA) (Millipore, #810683)]. The supernatant (ACM) was then collected, centrifuged at $500 \times g$ for 10 min at 4 °C, sterile filtered using a 22-μm filter, and stored at −80 °C.

RNA Sequencing and Processing. RNA was extracted with a GenElute Mammalian Total RNA Miniprep Kit (Sigma-Aldrich, #PLN70) according to the manufacturer's instructions. Sequencing libraries were prepared using the MARS-seq protocol (80). Libraries were normalized, pooled, and sequenced on a single lane of an Illumina NovaSeq. Poly-A/T stretches and Illumina adapters were trimmed from the reads using cutadapt, and resulting reads shorter than 30 bp were discarded. The remaining reads were mapped onto 3′ UTR regions (1,000 bases) of the *Mus musculus*, mm10 genome according to Refseq annotations, using STAR (81) with the EndToEnd option and with outFilterMismatchNoverLmax set to 0.05. Deduplication was accomplished by flagging all reads mapped to the same gene and had the same Unique Molecular Identifier (UMI). Raw read counts were normalized using the DESeq2 R package (82). Differentially expressed genes were identified using the DESeq2 package, with an adjusted P value of <0.05. IPA software (Qiagen) was used to identify regulators of gene expression networks by inputting gene expression datasets with corresponding log(fold change) expression levels compared to other groups. Canonical pathway metrics were considered significant at $P < 0.05$. Chea and JASPAR-TRANSFAC databases were accessed through the online open-access Enrichr platform (58). Resource database output files were then streamlined to leave only statistically enriched Transcriptional regulator IDs (Enrichr adjusted $P < 0.05$). Heatmaps were generated using the Morpheus portal of the Broad Institute (https://software.broadinstitute.org/morpheus).

CD38 Enzymatic Activity Assay (ε-NAD). CD38 activity was measured using the nicotinamide $1,N^6$-ethenoadenine dinucleotide (ε-NAD) fluorescence-based enzymatic assay, as described previously (83). Primary astrocyte cells were incubated with ε-NAD (40 μM; Sigma, N5131) in an extracellular solution of Hanks' Balanced Salt solution (HBSS) with Ca^{+2}/Mg^{+2}. Following a 15-min incubation, fluorescence was read at $\lambda_{Ex} = 300$ nm and $\lambda_{Em} = 410$ nm using a fluorescence microplate reader (Synergy HT, BioTek). The fluorescent readings were then normalized to viable cell numbers as determined by the AlamarBlue assay (Bio-Rad, #BUF012B). Normalized values are presented as CD38 activity.

Isolation and FACS Analysis of Adult Mice CNS Cells. Naïve and EAE mice were killed and subjected to perfusion through the left ventricle with ice-cold sterile PBS. Brains and spinal cords were then removed, minced, and enzymatically dissociated with 0.05% (wt/vol) collagenase type III (Worthington Biochemical, #LS004182), 0.5% Dispase II (Roche Applied Science, #4942078001), 40 μg/mL DNase I, 20 mM Hepes in HBSS) for 30 min at 37 °C to make a single-cell suspension. Enzymes were inactivated with 20 mL of Ca^{2+}/Mg^{2+}-free HBSS containing 2 mM Ethylenediaminetetraacetic acid (EDTA) and 20 mM Hepes. The digested tissue was triturated and passed through a 100-μM cell strainer. Cells were centrifuged and resuspended in 30% isotonic Percoll Plus (GE Healthcare, #17-5445-01) and 40 μg/mL DNase I, underlayered by 70% isotonic Percoll, and centrifuged at $1,000 \times g$ at 4 °C for 25 min. Cells were collected from the 70 to 30% interphase and analyzed by FACS using fluorochrome-conjugated antibodies. Monocyte recruitment was assessed by monitoring CD11b (M1/70, eBioscience, #48-0112-82) and CD45 (30-F11, Biolegend, #103113). The CD38 expression on astrocytes was measured using CD38 mAb (90, Biolegend, #102712 or #102708) in an astrocyte-enriched population (following the exclusion of lymphocytes, microglia, monocytes, and oligodendrocytes, as we described previously (2, 42).

Statistical Analysis. All samples were randomly allocated into treatment groups. No statistical methods were used to predetermine the sample size, which was chosen in accordance with previous studies in the field (2, 3, 6, 17, 44). In all cases, data are shown as mean ± SEM unless otherwise indicated. Statistical analyses were performed with Prism 9.3.1 software (GraphPad), and the statistical tests used are indicated in the individual figure legends. $P < 0.05$ was considered statistically significant.

Data, Materials, and Software Availability. RNA sequencing data supporting this study's findings have been deposited in the National Center for Biotechnology Information (NCBI) Gene Expression Omnibus(GEO) public repository (GSE205943 and GSE205944) (84, 85). Data from Schirmer et al. (62) were accessed at PRJNA544731 and https://cells.ucsc.edu/?ds=ms using the Xena platforms (86). Data from Zhang et al. (38, 61) were accessed via http://www.brainrnaseq.org/. Data from Saunders et al. (39) were accessed at GEO database under accesion number GSE116470 and http://www.dropviz.org/. Data from Russ et al. (40) and Matson et al. (41) were accessed via https://seqseek.ninds.nih.gov/home. Data from Rothhammer et al. (21) were accessed at https://figshare.com/s/e99974829c4d11e5a57b06ec4b8d1f61. All other study data are included in the article and/or supporting information.

ACKNOWLEDGMENTS. This work was supported by grants 963/16, 293/17, and 1564/20 from the Israel Science Foundation, and RG1611-26083 and RG1702-27015 from the National Multiple Sclerosis Society (to L.M.). We thank Drs. Alexander Brandis and Tevie Mehlman (Weizmann Institute of Science, Israel) for their assistance with the LC-MS/MS analysis. Illustrations were created with BioRender.com; a paid license of Biorender is available.

Author affiliations: [a]Sagol School of Neuroscience, Tel Aviv University, Tel Aviv 69978, Israel; [b]Shmunis School of Biomedicine and Cancer Research, George S. Wise Faculty of Life Sciences, Tel Aviv University, Tel Aviv 69978, Israel; and [c]Department of Neurology and Neurological Sciences, Beckman Center for Molecular Medicine, Stanford University School of Medicine, Stanford, CA 94305-5316

1. C. Baecher-Allan, B. J. Kaskow, H. L. Weiner, Multiple sclerosis: Mechanisms and immunotherapy. *Neuron* **97**, 742–768 (2018).
2. L. Mayo *et al.*, Regulation of astrocyte activation by glycolipids drives chronic CNS inflammation. *Nat. Med.* **20**, 1147–1156 (2014).
3. C.-C. Chao *et al.*, Metabolic control of astrocyte pathogenic activity via cPLA2-MAVS. *Cell* **179**, 1483–1498.e22 (2019).
4. A. Wagner *et al.*, Metabolic modeling of single Th17 cells reveals regulators of autoimmunity. *Cell* **184**, 4168–4185.e21 (2021).

5. P. Bhargava *et al.*, Bile acid metabolism is altered in multiple sclerosis and supplementation ameliorates neuroinflammation. *J. Clin. Invest.* **130**, 3467–3482 (2020).
6. S. G. Tullius *et al.*, NAD+ protects against EAE by regulating CD4+ T-cell differentiation. *Nat. Commun.* **5**, 5101 (2014).
7. H. A. Ferris *et al.*, Loss of astrocyte cholesterol synthesis disrupts neuronal function and alters whole-body metabolism. *Proc. Natl. Acad. Sci. U.S.A.* **114**, 1189–1194 (2017).
8. N. J. Allen, C. Eroglu, Cell biology of astrocyte-synapse interactions. *Neuron* **96**, 697–708 (2017).
9. Z. Zhao, A. R. Nelson, C. Betsholtz, B. V. Zlokovic, Establishment and dysfunction of the blood-brain barrier. *Cell* **163**, 1064–1078 (2015).
10. J. E. Burda *et al.*, Divergent transcriptional regulation of astrocyte reactivity across disorders. *Nature* **606**, 557–564 (2022).
11. M. Linnerbauer, M. A. Wheeler, F. J. Quintana, Astrocyte crosstalk in CNS inflammation. *Neuron* **108**, 608–622 (2020).
12. R. Perelroizen *et al.*, Astrocyte immunometabolic regulation of the tumour microenvironment drives glioblastoma pathogenicity. *Brain* (2022).
13. H. Wang *et al.*, Regulation of beta-amyloid production in neurons by astrocyte-derived cholesterol. *Proc. Natl. Acad. Sci. U.S.A.* **118**, e2102191118 (2021).
14. M. A. Wheeler *et al.*, MAFG-driven astrocytes promote CNS inflammation. *Nature* **578**, 593–599 (2020).
15. E. Verdin, NAD^+ in aging, metabolism, and neurodegeneration. *Science* **350**, 1208–1213 (2015).
16. S. Chowdhry *et al.*, NAD metabolic dependency in cancer is shaped by gene amplification and enhancer remodelling. *Nature* **569**, 570–575 (2019).
17. A. M. Cameron *et al.*, Inflammatory macrophage dependence on NAD+ salvage is a consequence of reactive oxygen species–mediated DNA damage. *Nat. Immunol.* **20**, 420–432 (2019).
18. N. Xie *et al.*, NAD^+ metabolism: Pathophysiologic mechanisms and therapeutic potential. *Signal Transduct. Target. Ther.* **5**, 227 (2020).
19. F. Wilhelm, J. Hirrlinger, Multifunctional roles of NAD+ and NADH in astrocytes. *Neurochem. Res.* **37**, 2317–2325 (2012).
20. A. Garten *et al.*, Physiological and pathophysiological roles of NAMPT and NAD metabolism. *Nat. Rev. Endocrinol.* **11**, 535–546 (2015).
21. V. Rothhammer *et al.*, Type I interferons and microbial metabolites of tryptophan modulate astrocyte activity and CNS inflammation via the aryl hydrocarbon receptor. *Nat. Med.* **22**, 586–597 (2016).
22. M. Platten, E. A. A. Nollen, U. F. Röhrig, F. Fallarino, C. A. Opitz, Tryptophan metabolism as a common therapeutic target in cancer, neurodegeneration and beyond. *Nat. Rev. Drug Discov.* **18**, 379–401 (2019).
23. G. Sundaram, C. K. Lim, B. J. Brew, G. J. Guillemin, Kynurenine pathway modulation reverses the experimental autoimmune encephalomyelitis mouse disease progression. *J. Neuroinflammation* **17**, 176 (2020).
24. C. A. Opitz, W. Wick, L. Steinman, M. Platten, Tryptophan degradation in autoimmune diseases. *Cell. Mol. Life Sci.* **64**, 2542–2563 (2007).
25. F. Sahm *et al.*, The endogenous tryptophan metabolite and NAD+ precursor quinolinic acid confers resistance of gliomas to oxidative stress. *Cancer Res.* **73**, 3225–3234 (2013).
26. G. A. Dienel, Brain glucose metabolism: Integration of energetics with function. *Physiol. Rev.* **99**, 949–1045 (2019).
27. A. A. Polyzos *et al.*, Metabolic reprogramming in astrocytes distinguishes region-specific neuronal susceptibility in Huntington mice. *Cell Metab.* **29**, 1258–1273.e11 (2019).
28. X.-Y. Xiong, Y. Tang, Q.-W. Yang, Metabolic changes favor the activity and heterogeneity of reactive astrocytes. *Trends Endocrinol. Metab.* **33**, 390–400 (2022).
29. W. Fu, D. Shi, D. Westaway, J. H. Jhamandas, Bioenergetic mechanisms in astrocytes may contribute to amyloid plaque deposition and toxicity. *J. Biol. Chem.* **290**, 12504–12513 (2015).
30. P. Kabiraj *et al.*, Teriflunomide shifts the astrocytic bioenergetic profile from oxidative metabolism to glycolysis and attenuates TNFα-induced inflammatory responses. *Sci. Rep.* **12**, 3049 (2022).
31. J. Muri, M. Kopf, Redox regulation of immunometabolism. *Nat. Rev. Immunol.* **21**, 363–381 (2021).
32. N. M. Chapman, H. Chi, Metabolic adaptation of lymphocytes in immunity and disease. *Immunity* **55**, 14–30 (2022).
33. M. D. Buck, R. T. Sowell, S. M. Kaech, E. L. Pearce, Metabolic instruction of immunity. *Cell* **169**, 570–586 (2017).
34. P. Marchetti, Q. Fovez, N. Germain, R. Khamari, J. Kluza, Mitochondrial spare respiratory capacity: Mechanisms, regulation, and significance in non-transformed and cancer cells. *FASEB J.* **34**, 13106–13124 (2020).
35. T. A. van Wageningen *et al.*, Distinct gene expression in demyelinated white and grey matter areas of patients with multiple sclerosis. *Brain Commun.* **4**, fcac005 (2022).
36. M. R. Langley *et al.*, Critical role of astrocyte NAD^+ glycohydrolase in myelin injury and regeneration. *J. Neurosci.* **41**, 8644–8667 (2021).
37. J. Roboon *et al.*, Deletion of CD38 suppresses glial activation and neuroinflammation in a mouse model of demyelination. *Front. Cell. Neurosci.* **13**, 258 (2019).
38. Y. Zhang *et al.*, An RNA-sequencing transcriptome and splicing database of glia, neurons, and vascular cells of the cerebral cortex. *J. Neurosci.* **34**, 11929–11947 (2014).
39. A. Saunders *et al.*, Molecular diversity and specializations among the cells of the adult mouse brain. *Cell* **174**, 1015–1030.e16 (2018).
40. D. E. Russ *et al.*, A harmonized atlas of mouse spinal cord cell types and their spatial organization. *Nat. Commun.* **12**, 5722 (2021).
41. K. J. E. Matson *et al.*, A single cell atlas of spared tissue below a spinal cord injury reveals cellular mechanisms of repair. *Biorxiv*, 2021.04.28.441862 (2021).
42. L. Mayo *et al.*, IL-10-dependent Tr1 cells attenuate astrocyte activation and ameliorate chronic central nervous system inflammation. *Brain* **139**, 1939–1957 (2016).
43. P. Aksoy, T. A. White, M. Thompson, E. N. Chini, Regulation of intracellular levels of NAD: A novel role for CD38. *Biochem. Biophys. Res. Commun.* **345**, 1386–1392 (2006).
44. S. Partida-Sánchez *et al.*, Cyclic ADP-ribose production by CD38 regulates intracellular calcium release, extracellular calcium influx and chemotaxis in neutrophils and is required for bacterial clearance in vivo. *Nat. Med.* **7**, 1209–1216 (2001).
45. T. M. Ross *et al.*, Intranasal administration of interferon beta bypasses the blood-brain barrier to target the central nervous system and cervical lymph nodes: A non-invasive treatment strategy for multiple sclerosis. *J. Neuroimmunol.* **151**, 66–77 (2004).
46. M. Linnerbauer *et al.*, Intranasal delivery of a small-molecule ErbB inhibitor promotes recovery from acute and late-stage CNS inflammation. *JCI Insight* **7**, e154824 (2022).
47. M. Zhou *et al.*, Neuronal death induced by misfolded prion protein is due to NAD+ depletion and can be relieved in vitro and in vivo by NAD+ replenishment. *Brain* **138**, 992–1008 (2015).
48. W. Ying *et al.*, Intranasal administration with NAD+ profoundly decreases brain injury in a rat model of transient focal ischemia. *Front. Biosci.* **12**, 2728–2734 (2007).
49. C. Zheng *et al.*, NAD(+) administration decreases ischemic brain damage partially by blocking autophagy in a mouse model of brain ischemia. *Neurosci. Lett.* **512**, 67–71 (2012).
50. M. E. Deerhake *et al.*, Dectin-1 limits autoimmune neuroinflammation and promotes myeloid cell-astrocyte crosstalk via Card9-independent expression of Oncostatin M. *Immunity* **54**, 484–498.e8 (2021).
51. Y. M. Khaw *et al.*, Astrocytes lure CXCR2-expressing $CD4^+$ T cells to gray matter via TAK1-mediated chemokine production in a mouse model of multiple sclerosis. *Proc. Natl. Acad. Sci. U.S.A.* **118**, e2017213118 (2021).
52. A. Mildner *et al.*, CCR2+Ly-6Chi monocytes are crucial for the effector phase of autoimmunity in the central nervous system. *Brain* **132**, 2487–2500 (2009).
53. M. Moreno *et al.*, Conditional ablation of astroglial CCL2 suppresses CNS accumulation of M1 macrophages and preserves axons in mice with MOG peptide EAE. *J. Neurosci.* **34**, 8175–8185 (2014).
54. M. Howard *et al.*, Formation and hydrolysis of cyclic ADP-ribose catalyzed by lymphocyte antigen CD38. *Science* **262**, 1056–1059 (1993).
55. S. Partida-Sánchez *et al.*, Regulation of dendritic cell trafficking by the ADP-ribosyl cyclase CD38 impact on the development of humoral immunity. *Immunity* **20**, 279–291 (2004).
56. A. H. Guse *et al.*, Regulation of calcium signalling in T lymphocytes by the second messenger cyclic ADP-ribose. *Nature* **398**, 70–73 (1999).
57. L. Mayo *et al.*, Dual role of CD38 in microglial activation and activation-induced cell death. *J. Immunol.* **181**, 92–103 (2008).
58. M. V. Kuleshov *et al.*, Enrichr: A comprehensive gene set enrichment analysis web server 2016 update. *Nucleic Acids Res.* **44** (W1), W90–W97 (2016).
59. J. L. Furman *et al.*, Targeting astrocytes ameliorates neurologic changes in a mouse model of Alzheimer's disease. *J. Neurosci.* **32**, 16129–16140 (2012).
60. M. R. Müller, A. Rao, NFAT, immunity and cancer: A transcription factor comes of age. *Nat. Rev. Immunol.* **10**, 645–656 (2010).
61. Y. Zhang *et al.*, Purification and characterization of progenitor and mature human astrocytes reveals transcriptional and functional differences with mouse. *Neuron* **89**, 37–53 (2016).
62. L. Schirmer *et al.*, Neuronal vulnerability and multilineage diversity in multiple sclerosis. *Nature* **573**, 75–82 (2019).
63. M. H. A. Roehrl *et al.*, Selective inhibition of calcineurin-NFAT signaling by blocking protein-protein interaction with small organic molecules. *Proc. Natl. Acad. Sci. U.S.A.* **101**, 7554–7559 (2004).
64. P. Sompol *et al.*, Calcineurin/NFAT signaling in activated astrocytes drives network hyperexcitability in Aβ-bearing mice. *J. Neurosci.* **37**, 6132–6148 (2017).
65. B. A. C. Cree *et al.*, Secondary progressive multiple sclerosis: New insights. *Neurology* **97**, 378–388 (2021).
66. B. Styr *et al.*, Mitochondrial regulation of the hippocampal firing rate set point and seizure susceptibility. *Neuron* **102**, 1009–1024.e8 (2019).
67. A. E. Miller, Oral teriflunomide in the treatment of relapsing forms of multiple sclerosis: Clinical evidence and long-term experience. *Ther. Adv. Neurol. Disord.* **10**, 381–396 (2017).
68. J. Correale, M. I. Gaitán, M. C. Ysrraelit, M. P. Fiol, Progressive multiple sclerosis: From pathogenic mechanisms to treatment. *Brain* **140**, 527–546 (2017).
69. A. Levy *et al.*, CD38 deficiency in the tumor microenvironment attenuates glioma progression and modulates features of tumor-associated microglia/macrophages. *Neuro-oncol.* **14**, 1037–1049 (2012).
70. A. Levy *et al.*, CD38 facilitates recovery from traumatic brain injury. *J. Neurotraum.* **26**, 1521–1533 (2009).
71. M. Li *et al.*, Local targeting of NAD^+ salvage pathway alters the immune tumor microenvironment and enhances checkpoint immunotherapy in glioblastoma. *Cancer Res.* **80**, 5024–5034 (2020).
72. N. Baum *et al.*, Mouse CD38-specific heavy chain antibodies inhibit CD38 GDPR-cyclase activity and mediate cytotoxicity against tumor cells. *Front. Immunol.* **12**, 703574 (2021).
73. S. Kaneko *et al.*, Protecting axonal degeneration by increasing nicotinamide adenine dinucleotide levels in experimental autoimmune encephalomyelitis models. *J. Neurosci.* **26**, 9794–9804 (2006).
74. T. V. Lanz *et al.*, Clonally expanded B cells in multiple sclerosis bind EBV EBNA1 and GlialCAM. *Nature* **603**, 321–327 (2022).
75. Y. Liu *et al.*, Reduced nicotinamide mononucleotide (NMNH) potently enhances NAD^+ and suppresses glycolysis, the TCA cycle, and cell growth. *J. Proteome Res.* **20**, 2596–2606 (2021).
76. L. Kalikin, K. C. Calvo, Inhibition of quinolinate phosphoribosyl transferase by pyridine analogs of quinolinic acid. *Biochem. Biophys. Res. Commun.* **152**, 559–564 (1988).
77. J. Saura, J. M. Tusell, J. Serratosa, High-yield isolation of murine microglia by mild trypsinization. *Glia* **44**, 183–189 (2003).
78. N. Braidy, M. D. Villalva, R. Grant, NADomics: Measuring NAD^+ and related metabolites using liquid chromatography mass spectrometry. *Life (Basel)* **11**, 512 (2021).
79. P. Lu *et al.*, Poly(ADP-ribose) polymerase-1 inhibits mitochondrial respiration by suppressing PGC-1α activity in neurons. *Neuropharmacology* **160**, 107755 (2019).
80. H. Keren-Shaul *et al.*, MARS-seq2.0: An experimental and analytical pipeline for indexed sorting combined with single-cell RNA sequencing. *Nat. Protoc.* **14**, 1841–1862 (2019).
81. A. Dobin *et al.*, STAR: Ultrafast universal RNA-seq aligner. *Bioinformatics* **29**, 15–21 (2013).
82. M. I. Love, W. Huber, S. Anders, Moderated estimation of fold change and dispersion for RNA-seq data with DESeq2. *Genome Biol.* **15**, 550 (2014).
83. G. C. de Oliveira, K. S. Kanamori, M. Auxiliadora-Martins, C. C. S. Chini, E. N. Chini, Measuring CD38 hydrolase and cyclase activities: $1,N^6$-ethenonicotinamide adenine dinucleotide (ε-NAD) and nicotinamide guanine dinucleotide (NGD) fluorescence-based methods. *Bio Protoc.* **8**, e2938 (2018).
84. L. Mayo, Effect of NAMPT inhibition on gene expression in LPS/IFNg-stimulated primary mouse astrocytes. NCBI Gene Expression Omnibus. https://www.ncbi.nlm.nih.gov/geo/query/acc.cgi?acc=GSE205944. Deposited 12 June 2022.
85. L. Mayo, Effect of depletion of CD38 on gene expression in LPS/IFNg-stimulated primary mouse astrocytes. NCBI Gene Expression Omnibus. https://www.ncbi.nlm.nih.gov/geo/query/acc.cgi?acc=GSE205943. Deposited 12 June 2022.
86. M. J. Goldman *et al.*, Visualizing and interpreting cancer genomics data via the Xena platform. *Nat. Biotechnol.* **38**, 675–678 (2020).
87. S. Lautrup, D. A. Sinclair, M. P. Mattson, E. F. Fang, NAD^+ in brain aging and neurodegenerative disorders. *Cell Metab.* **30**, 630–655 (2019).